Fast and ample light controlled actuation of monodisperse all-DNA microgels

Rémi Merindol,[a] Nicolas Martin,[b] Thomas Beneyton, [b] Jean-Christophe Baret,[b,c] and Serge Ravaine[b]*

Dr. R. Merindol
Univ. Montpellier, CNRS, L2C UMR 5221
Place Eugène Bataillon,
34000 Montpellier, France
remi.merindol@umontpellier.fr

Dr. N. Martin, Dr. T. Beneyton, Prof. J.C. Baret, Prof. S. Ravaine
Univ. Bordeaux, CNRS, CRPP UMR 5031
115 Avenue du Dr Albert Schweitzer,
33600 Pessac, France

Prof. J.C. Baret
Institut Universitaire de France,
75005 Paris, France

This is the last submitted version of the manuscript published as:

Fast and ample light controlled actuation of monodisperse all-DNA microgels
https://doi.org/10.1002/adfm.202010396

for publication on institutional deposits.

Abstract

The assembly of adaptive hierarchical soft-materials that resemble living tissues requires responsive building blocks of controlled dimensions. While DNA self-assembly provides an exceptional tool for nanoscale architectural control, responsive DNA microstructures remain scarce. Here, we address two challenges controlling the size of DNA microstructures and embedding them with fast and ample structural response. For size-control, we combine arrested phase separation and microfluidic confinement to produce monodisperse all-DNA particles. For responsiveness we implement a light controlled coil-globule transition of the microgel DNA network powered by an azobenzene cationic surfactant. The photoinduced trans-cis isomerization of the azobenzene moiety reduces its affinity for DNA which results in fast, large amplitudes microgel swelling. Finally we demonstrate the assembly of light responsive periodic microgel lattices as proof-of-concept hierarchical all-DNA materials.

1. Introduction

Biological materials consist of hierarchical assemblies of biomolecules that constantly sense and interact with their environment.[1,2] Reproducing such an adaptive multi-scale organization is attracting growing interest to build life-inspired materials.[3] Hydrogels and microgels that dynamically respond to external cues across length scales are particularly crucial for cell studies and tissue engineering.[4–6] The bottom-up construction of such dynamic hierarchical materials requires the design of building blocks with the highest number of orthogonal control over their geometry, interactions, functionalization sites and responsive properties.

DNA is the best example of such versatile building blocks at the molecular scale.[7] DNA self-assembly provides artificial materials with molecular structural control (*e.g.* DNA origami…),[8] easy functionalization with multiple DNA labelled probes[9] and programmable dynamic behaviour with enzymatic[10,11] and strand displacement reactions.[12] DNA-based

materials also naturally respond to various stimuli, including heat,[13] pH,[14,15] metal ions[16] or biomolecules.[17] This set of orthogonal control offers a robust and modular platform to develop personalized medicine,[18] study cell behaviour,[5] and mimic biological non-equilibrium processes.[19]

Recent works on DNA self-assembly target a structural control at always larger length scales towards micrometric objects[20,21] and macroscale materials.[22] Yet, sequence-driven self-assembly of individual DNA molecules into defined superstructures becomes slow and difficult at the micron scale as the number of accessible microstates increases exponentially. Mesoscale building blocks offer a convenient way to speed up the assembly of hierarchically structured materials.[6] Phase transitions in polyelectrolyte solutions provides means to spontaneously prepare such mesoscale structures.[23,24] When combined to microfluidics, the structures are highly controlled as exemplified with DNA solutions producing liquid micro-compartments[25] or with the preparation of crystalline particles of clonal DNA sequences.[26,27] We recently combined DNA liquid-liquid phase separation and supramolecular hybridization to explore new assembly landscapes for the pathway controlled formation of mesoscale all-DNA microgels.[28] However, the arrested phase separation at the origin of these DNA colloids yielded highly polydisperse particles, which prevented their assembly into well-defined superstructures.[29,30] Developing monodisperse all-DNA microgels represents a crucial step to assemble exotic photonic superstructures [29,30] and embed them with responsive properties,[31] or produce hierarchical soft materials that can adapt and process signals.[32,33]

Beyond structural control, there is a growing interest to design responsive DNA. Owing to its great spatiotemporal capability, light is the most promising trigger for such a purpose. For instance, azobenzene photoswitches grafted onto DNA chains were used to promote volume changes of hybrid DNA-polymer hydrogels in response to light due to photoreversible DNA hybridization.[34] Yet, as opposed to fully synthetic polymer microgels whose radii easily double or triple upon irradiation due to coil-globule transition,[35] hybrid polymer-DNA hydrogels

display small volume changes because the azobenzene groups only impact the DNA crosslinks and not the full hydrogel network.[15,34] Other example of responsive DNA microgels either burst open upon photothermal trigger,[28] dissolve due to enzymatic degradation,[36] swell due to metaloenzyme catalysed polymerization,[32] or grow irreversibly with the insertion of DNA hairpins.[37,38] As opposed to the rich diversity of responsive synthetic microgels driven by coil-globule transition,[39] we lack DNA microstructures with fast and ample structural response.

Here, we report the formation of monodisperse all-DNA microgels of controllable size via droplet-based microfluidics, and show that a cationic azobenzene photoswitch (azobenzenetrimethyl-ammonium bromide, azoTAB) promotes fast, large and reversible volume changes of the microgels upon light irradiation. This light-actuated swelling and compaction process arises from *trans-cis* photoisomerisation of azoTAB that impacts its binding affinity to DNA chains and induces globule-coil transition of the backbone conformation.[40–42] We further report self-assembly of the monodisperse photoresponsive DNA microgels into regular superstructures as a step towards light adaptive hierarchical DNA materials that can undergo large scale structural reconfigurations. Our results describe an efficient approach to design size-controlled photoresponsive DNA microstructures as versatile building block for the assembly of responsive biomaterials.

2. Assembly of monodisperse all-DNA microgels

All-DNA microgels were produced by arrested phase separation of long single-stranded DNA (ssDNA), obtained by rolling circle amplification (RCA) of a circularized template with φ29 polymerase, in the presence of divalent counterions, as reported previously.[28] (Figure S1) We here used a template consisting of (i) a 20 bases long homo-adenine run that promotes phase separation at high temperature in the presence of magnesium or calcium counterions, (ii) a self-complementary (palindromic) domain that forms duplexes upon cooling, therefore stabilizing the DNA-rich phase into soft microgels, and (iii) a recognition (bar-code) domain that remains

single stranded and serves as an addressable anchor that can be labelled using fluorescent oligonucleotides (Figure S2). In bulk, the arrested phase separation produced polydisperse microgels (Figure S2) due to uncontrolled coalescence and ripening of DNA-rich droplets formed upon heating, as observed previously. We therefore developed a procedure to form monodisperse all-DNA microgels using droplet-based microfluidics (**Figure 1a**). Surfactant-stabilized monodiperse water-in-oil drops of diameter D_{Drop} = 35 µm encapsulating a homogeneous solution of long ssDNA and calcium ions (50 mM $CaCl_2$) were first produced using a flow-focusing microfluidic device (Figure 1b and Figure S3). Liquid-liquid DNA phase separation within the microfluidic emulsion drops was then induced by thermal treatment at 85°C for 2 h. During this incubation time, we observed the nucleation of small DNA-rich droplets and their fusion into a larger single micro-droplet (Figure S4 for short incubation time). Cooling down to room temperature induced gelling of the phase-separated DNA droplets to produce a single microgel per droplet (Figure 1c). We can estimate the fluctuation of concentrations as the square-root of the number of DNA molecules per drop, in our system these variations fall between 7 % at 3 $mg.L^{-1}$ and 1 % at 100 $mg.L^{-1}$ (taking 200 $kg.mol^{-1}$ as average molecular weight). Since each droplet initially contains similar amount of DNA, phase separation results in microgels with similar size. The final step consisted in destabilizing the microfluidic emulsion to remove the oil phase and collect the microgels by centrifugation. The collected microgels were monodisperse (Figure 1d), as expected from the narrow distribution of the number of DNA per droplet, and could be re-dispersed into the desired buffer for downstream applications.

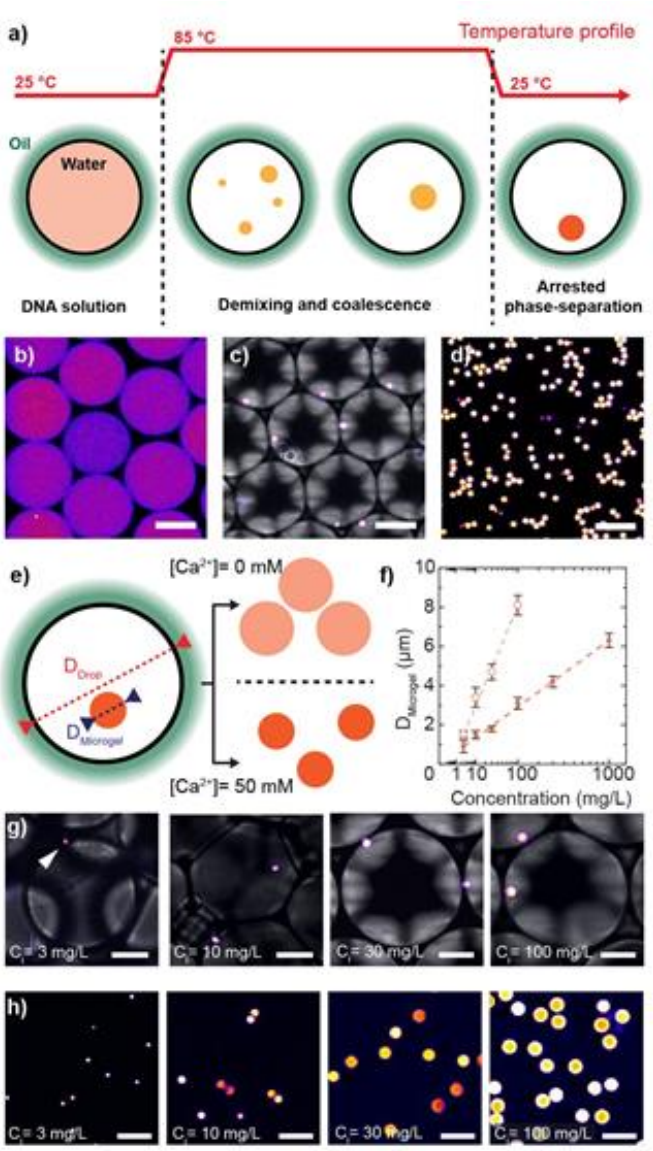

Figure 1. Preparation of monodisperse DNA microgels via arrested phase-separation in microfluidic confinement. a) Schematic representation of the confined phase separation yielding monodisperse DNA microgels. b-d) Confocal laser scanning micrographs (CLSM) at different stages of the process. b) Homogeneous DNA solution in the microfluidic emulsion before heating. c) Individual microgels in the emulsion after phase separation. d) Monodisperse microgels gathered after destabilization of the emulsion. e) Schematic representation of the confined microgels and purified objects dispersed in low and high ionic strength solution. f) Graph presenting the diameter of the final microgels as function of the initial DNA concentration. Open circle correspond to the swollen diameter measured in TE and the filled dot correspond to the microgels in 50 mM $CaCl_2$. Note that the data are plotted with a cubic-root scales as x-axis. g) Superposition of CLSM and transmission optical micrographs showing the microgels as prepared from different initial DNA concentrations in their microfluidic emulsion. h) CLSM showing the purified microgels in TE. We used "Fire" look-up-table from ImageJ to show fluorescence through the manuscript. Error bars on f) represent standard deviation from the average value measured on at least 20 microgels. Scale bars, b-d) 20 µm and g,h) 10 µm.

We systematically investigated the relation between the initial DNA concentration in the homogeneous solution and the diameter of the DNA microgels both in the calcium solution (50 mM $CaCl_2$) and at lower ionic strength in Tris-EDTA (TE) buffer (10 mM Tris, 1 mM EDTA) (Figure 1e-h). As expected, the microgel diameter increased with increasing initial DNA concentration. The DNA microgels also exhibited a larger diameter at lower ionic strength, up to 3.2 times the initial diameter corresponding to a 33-fold volume increase, consistent with swelling due to enhanced electrostatic repulsion between DNA strands. We further observed that the microgel diameter grew linearly with the cubic root of the initial DNA concentration (Figure 1f). If we assume that all the DNA strands initially present in one microfluidic drop end up in the final microgel, we can fit the data using **Equation 1**, which gives the diameter of the DNA microgel ($D_{microgel}$) as function of the initial microfluidic drop diameter (D_{Drop}), initial DNA concentration (C_i) and the DNA concentration in the microgel (ρ_{DNA}). Our microfluidic drops were 35 µm in diameter and we measured 0.63 ± 0.03 µm·L·mg^{-1} and 2.0 ± 0.1 µm·L·mg^{-1} for the slope of the linear fit of particles respectively in the calcium solution and in TE buffer. The DNA content in the microgels was therefore calculated to be 17 ± 2 wt% in Ca^{2+} and 0.53 ± 0.8 wt% in TE buffer, respectively. Although we considered the possibility that some DNA remained in solution after thermal treatment, the linear fit in Figure 1g crosses the abscissa very close to the origin (at a concentration below 0.01 mg.L^{-1}), which suggests that the remaining DNA in solution is negligible in this case. We were yet unable to observe the formation of DNA microgels below 3 mg.L^{-1} of total DNA concentration.

$$\boldsymbol{D_{microgel} = D_{Drop} * \sqrt[3]{\frac{C_i}{\rho_{DNA}}}} \qquad \text{(Equation 1)}$$

3. Light controlled actuation

The above observations exemplify the high volume change capability of the monodisperse all-DNA microgels. Here we demonstrate that we can use a cationic azoTAB photoswitch (**Figure 2a**) to control this process. AzoTAB has previously been exploited for the reversible photocontrol of DNA coil-globule transition and coacervation in solution.[40–43] Addition of *trans*-azoTAB at concentrations above 1 mM to monodisperse all-DNA microgels prepared at 100 mg.mL^{-1} and suspended in TE buffer induced a significant microgel compaction (Figure 2b and Figure S5), with a maximum ~2.6-fold decrease in the microgel diameter, corresponding to a ~17-fold volume decrease. In comparison, UV-adapted *cis*-azoTAB did not impact significantly the microgel size on the whole range of concentrations tested (Figure 2b), so that irradiation of the dark-adapted microgels with UV light in the presence of 3 mM *trans*-azoTAB resulted in significant microgel swelling due to *trans*-*cis* azoTAB photoisomerisation (Figure 2a,c and Figure S5). Reversibly, blue light irradiation favoured the compaction of the UV-adapted microgels due to *cis*-*trans* azoTAB photoisomerisation (Figure 2a,c). This light-actuated swelling/compaction process could be repeated over multiple UV/blue-light irradiation cycles without any apparent fatigue (Figure 2c).

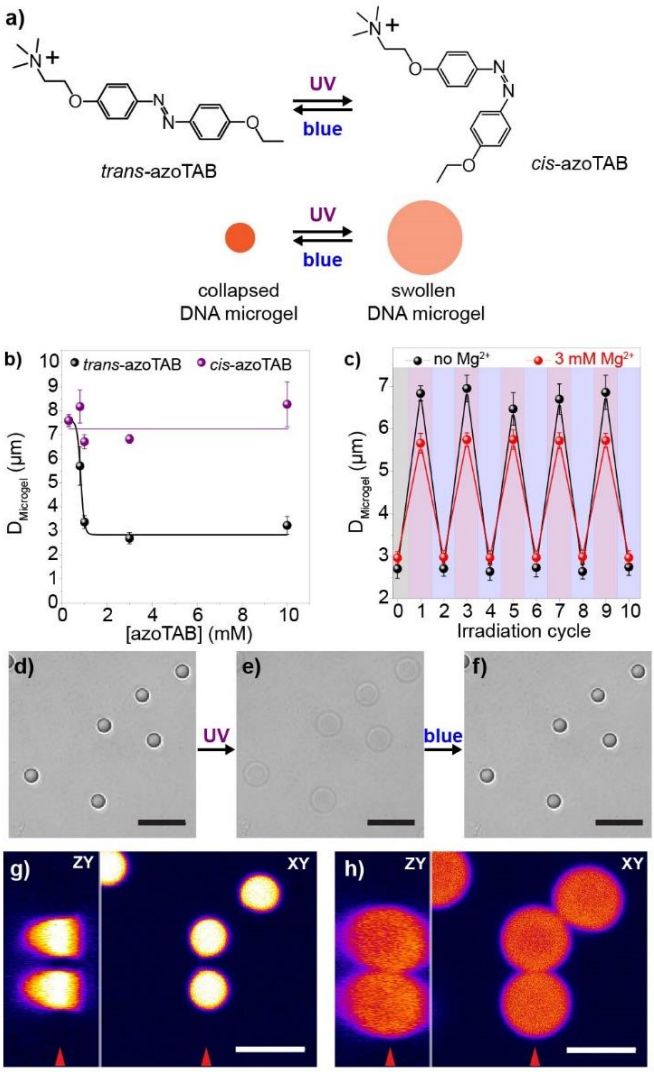

Figure 2. Photoresponsive DNA microgels using azobenzene surfactants. a) Molecular structure of the two conformation of azobenzenetrimethylammonium bromide (azoTAB) and the corresponding state of the DNA microgels. b) Graph presenting the diameter of DNA microgels prepared at 100 mg.L^{-1} in TE as function of the concentration of trans-(dark) or cis-(purple) azoTAB. c) Variation of the diameter of microgels in presence of 3 mM of AzoTAB, either with or without 3 mM Mg^{2+}, under 5 cycles of UV and blue light irradiation. d-f) optical micrographs and g,h) confocal laser scanning micrograph, showing swelling and deswelling of the DNA microgels (3mM AzoTAB, 4 mM $MgCl_2$) under UV (e,h) and blue light irradiation (d,f,g). The left panel of micrographs (g,h) present a ZY cut, and the right panel a XY cut. The position of the cut on each image is represented by a red arrow at the bottom. Error bars on b,c) represent standard deviation from the average value measured on 20 microgels from the same field of view. Scale bars d-f) 10 µm, and g,h) 5 µm.

Addition of magnesium ions decreased the light-driven microgel swelling capability (Figure 2c,d), as expected from screening of inter-DNA electrostatic repulsion at higher ionic strength (Figure S5), but more regular collapsed microgels were produced (Figure 2e) compared to low ionic strength conditions (Figure S5), consistent with higher reorganisation dynamics in the

presence of competing counterions.[43] In the following experiments, we thus chose to fix the concentration of magnesium ions to 3 mM to maintain a regular collapsed state while retaining a sufficiently large swelling ratio. In such conditions, optical microscopy revealed a ~2-fold change of the microgel diameter upon light irradiation, corresponding to a ~8-fold volume change (Figure 2d-f). The swelling process was typically completed within a few seconds (Movie S1), and the kinetics of the process could be modulated by varying the light intensity (Figure S6). Confocal fluorescence microscopy images of DNA microgels functionalized with fluorescently labelled complementary oligonucleotides confirmed that the light-actuated compaction and swelling process occurred in both xy and zy directions (Figure 2g,h and Movie S2). Significantly, the variation of fluorescence intensity within the microgels showed that the fluorophores followed the DNA network during compaction (higher fluorescence, Figure 2g) and swelling (lower fluorescence, Figure 2h), which indicated that supramolecular DNA hybridization was unaffected by the surfactant conformation, unlike what has been reported for azobenzene-grafted DNA strands.[34]

3. Responsive superstructures

We last investigated the assembly of all-DNA monodisperse microgels, to form photoresponsive superstructures. Although sequence controlled interaction between DNA-decorated colloids provides a powerful platform to elaborate complex materials, the narrow crystallisation range makes its implementation difficult.[29,44] Therefore, we relied here on a simpler strategy. We compacted the repulsive DNA colloids at low ionic strength by slow drying of a microgel suspension in TE buffer at room temperature. Slow water evaporation gradually concentrated the colloids, eventually leading to a compact periodic layer of microgels that was either immobilized onto the underlying glass coverslip surface (**Figure 3a-c**) or remained as a free-standing film (Figure 3d-i) depending on the rehydration protocol (See Methods). Similarly to dispersed microgels, in presence of TE buffer containing magnesium

ions (3 mM) and *trans*-azoTAB (3 mM) these microgel assembly are light responsive. We observed that the 5.4 ± 0.5 μm period of the compacted microgels immobilized onto the coverslip surface did not change during UV light irradiation (Figure 3a-c), as expected from the fixed position of the microgels. As a result, light-actuation swelling/deswelling of the immobilized microgel layer produced a reversible switch in the surface coverage from 55% (dark, collapsed microgels) to 85% (UV, swollen microgels)(Movie S3). In comparison, the lattice period of free standing microgel films could be reversibly photoswitched between ~3.6 μm (dark or blue light, Figure 3e) and ~5.2 μm (UV light, Figure 3f) due to light-actuated microgel swelling/deswelling. The period photoswitch was achieved in a few seconds, and could be repeated several times (Movie S4). Significantly, while we observed mostly homothetic transformations in small microgel assemblies (Figure 3e,f and Movie S4), larger pieces of self-assembled microgels tended to fold and twist, which resulted in large amplitude reconfigurations under UV light (Figure 3g-i and Movie S5). Although this goes beyond the scope of this communication, localized swelling could provide a general strategy to control non trivial motion mechanisms[45] (e.g. between light-responsive DNA microgels and passive DNA coated silica particles).

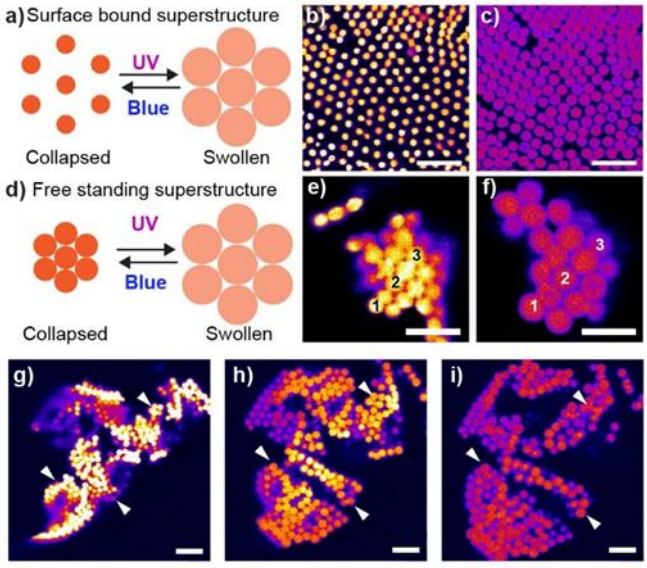

Figure 3. Photoresponsive microgels assemblies. a-c) Shematic representation a) and corresponding CLSM showing the photoinduced change of surface covered by an array of DNA microgels b,c). d-e) Shematic representation d) and corresponding CLSM of a small microgel

assembly whose period varies under light induced swelling. e,f). g-i) CLSM showing the large amplitude reorganisation of a large particle assemblies. All images are taken in TE with 3 mM $MgCl_2$ and 3 mM of AzoTAB, using Microgels prepared at 100 mg.L^{-1}. Scale bars for a-c and g-i, 20 µm and for d,e 10 µm.

3. Conclusions

These results show that all-DNA materials present fast and wide light-triggered swelling/compaction properties in the presence of a cationic azobenzene photoswitch. Such swelling, based on coil-globule transition in the hydrogel network, surpasses what has been reported in hybrid DNA-polymer hydrogels.[34] We demonstrated this effect using monodisperse all-DNA microgels and showed its transfer to the next structural level with the actuation of microgels superstructures. Since azoTAB has been used to control DNA transcription,[42] our results also provide new routes for light-controlled cell-free gene expression in DNA microgels.[46] Our microfluidic production process also improves on the previous microgel preparation protocols and enables the assembly of size-controlled DNA microgels with diameters that are one order of magnitude smaller than the microfluidic emulsion drops, thereby decreasing the size accessible by simple gelling of the whole drops' content.[47,48] We show that the improved size control of all-DNA microgels enables their assembly into periodic structures, which was impossible with the previously reported process.[28] Overall, our results offer new tools for the design of responsive DNA materials, opening perspectives for drug-delivery, nanomechanical devices and tissue engineering applications.

4 Experimental Section

4.1. Materials

ssDNA oligomers were purchased from EurogenTech as summarized in Table S1. The enzymes T_4 ligase (2.5 WU.µL^{-1}), Exonuclease I (20 U.µl^{-1}), Exonuclease III (200 U.µL^{-1}) as well as Deoxynucleotide triphosphate (dATP, dTTP, dGTP and dCTP) 100 µM were purchased from Jena bioscience. Φ_{29} polymerase (10 U.µL^{-1}) was purchased from Lucigen. Inorganic

pyrophosphatase (0.1 $U.\mu L^{-1}$) was bought from Thermofisher. Magnesium chloride anhydre ($MgCl_2$), Sodium chloride (NaCl), Calcium chloride ($CaCl_2$), tris(hydroxymethyl)aminomethane hydrochloride (TRIS-HCl and Trizma buffer substance pH=8), disodium ethylenediaminetetraacetate dihydrate (EDTA), mineral oil, Agarose Low EEO and TBE buffer 10X from Sigma-Aldrich. SYBR gold, loading dye, 10 bp ladder were purchased from ThermoFisher Scientific. Unless stated otherwise, the base of all solutions for particle preparation and assembly is a TE buffer that consists of 10 mM of Tris(hydroxymethyl)aminomethane (pH=8.0) and 1 mM of EDTA. DNA sequences are also stored frozen at -25°C in TE buffer. Gel electrophoresis (GEP) were run using 2 wt% Agarose gel in TBE buffer containing 89 mM of TRIS-HCl, 89 mM of boric Acid, 2 mM EDTA. Gels were post stained by soaking them in a SYBR gold diluted to 1X in a TBE buffer for 20 min.

AzoTAB was synthesized using a three-step reaction described previously by azocoupling *p*-ethoxyaniline with phenol, followed by alkylation with dibromoethane then quaternisation with trimethylamine.[43,49] PCB-mounted LEDs operating at 365 ± 4.5 nm (model M365D2) or 450 ± 9 nm (model M450D3) were purchased from Thorlabs, Inc. and adapted on a custom-made aluminium heat sink. The LEDs were controlled by a T-Cube LED driver that was purchased from Thorlabs, Inc.

Thermal ramps were performed on a thermocycler (T100, Bio-Rad), DNA concentrations were measured using a NanoDrop 2000 C (Fisher Scientific) spectrophotometer with a standard value of 33 $\mu g.OD_{260}^{-1}$. Confocal laser scanning microscopy (CLSM) was performed on Leica TCS SP2 microscope.

Table 1. Sequences used, with their name the purification grade and modifications.

	Name	Sequence 5'→3'	Purification	Modification
Templates for RCA	Tp_A[a]	ATC TAT CCT AA T TTT TTT TTT TTT TTT TTT T CG GAT GCG CAT CCG GAA CCC GTA T	HPLC	5'-Phosphorylation
	Tp_B[a]	CGCTG TGATC T TTT TTT TTT TTT TTT TTT TCG GAT GCG CAT CCG CGTTCGAGCA	HPLC	5'- Phosphorylation
Ligation strands	Lig_A	TTA GGA TAG ATA TAC G	HPLC	None
	Lig_B	CAG CGT GCT CGA ACG	HPLC	None
RCA Primers	Prim_A	TTA GGA TAG ATA TA*C*G	Desalting	Phosphorothioated Twice
	Prim_B	CAG CGT GCT CGA A*C*G	Desalting	Phosphorothioated Twice
Fluorescent oligomer	$Atto_{565}$-B	AAA ACC ACA CGA TCC TCT AAA A	HPLC	5' Atto 565 (NHS ester)

[a] These sequences are converted into polymers using RCA. Hence, the complementary nucleobase base structure is found in the multiblock copolymers.

4.2. DNA synthesis

The RCA process, schematized (Figure S1a), follows three main steps, the circularization of linear templates (I->II), the removal of unligated products(II->III) and the template amplification (IV). For circularization the linear template (100 µM in TE) and its corresponding ligation strands (100 µM in TE) are mixed to reach a final concentration of 5 µM in TE buffer containing additionally 100 mM NaCl (total 20 µL). The solution is heated up to 85°C and cooled down to 25°C at 0.5°C.min^{-1}. After hybridization 4 µL of 10 X commercial ligase buffer (Jena Bioscienc: 500 mM TRIS-HCI pH 7.8 at 25 °C, 100 mM $MgCl_2$, 100 mM dithiothreitol, 10 mM ATP and 25 $mg.ml^{-1}$ BSA), 14 µL of water and 2 µL of T_4 Ligase (2.5 $WU.\mu L^{-1}$) are introduced in the tube containing the template strand, gently mixed and left to react for 3 hours at room temperature. The enzyme is deactivated by heating the mixture for 20 min at 70°C.

Unligated products are removed using exonucleases that digest linear products from their extremities. The absence of "ends" in circularized DNA prevents their digestion. To this end, 2 µL of Exonuclease I (20 $U.\mu L^{-1}$) and 2 µL Exonuclease III (200 $U.\mu L^{-1}$) are introduced and the

mixture is left overnight at 37°C. The enzymes are then deactivated by heating at 80°C for 40 min. The templates are purified by filtration over Amicon Ultracentrifugal filters with a 10 kDa cut-off (Merck Millipore) and rinced 3 times using TE buffer in the same filter. The ssDNA concentrations are measured using a Nanodrop 2000C (Fisher scientific) and the solutions are diluted to 1 μM using TE buffer. A control experiments which followed exactly the same step as discussed above, except that the T4 DNA ligase was replaced by 2 μL of water, shows Figure S1b, that the enzyme can digest all the non-ligated DNA strands.

For RCA, 10 μL circularized template (1 μM) are mixed with 150 μL of ultrapure water, 2 μL of RCA primer (10 μM in TE buffer), 20 μL of commercial 10 X polymerase buffer (Lucigen: 500 mM TRIS-HCl, 100 mM $(NH_4)_2SO_4$, 40 mM Dithiothreitol, 100 mM $MgCl_2$), 4 μL of Φ_{29} Polymerase (10 $U.\mu L^{-1}$), 0.5 μL of pyrophosphatase (2 $U.\mu L^{-1}$). The mixture is left for 1 hour at room temperature in order to pre form the enzyme DNA complexes before addition of 10 μL of an adjusted dNTP mix (total dNTP concentration of 100 mM the proportion of each bases correspond to the expected product composition) to start the amplification reaction. The samples are kept for 48 hours at 30°C before inactivation for 10 min at 80°C. The product is then concentrated by filtration over Amicon Ultracentrifugal filters with a 30 kDa cut-off (Merck Millipore) and rinsed 3 times using 400 μL of TE buffer. The RCA product is rediluted into 50 μL of TE buffer, homogeneized at 95 °C for 10 min, the amount and purity of the ssDNA concentration are then measured using a Nanodrop 2000C (Fisher scientific) spectrophotometer using 33 $\mu g.OD_{260}^{-1}$ as standard absorbance coefficient for single stranded DNA.

4.3. Mechanism of the arrested phase separation

We used template A, through the manuscript to optimize the assembly conditions and control the mean particle diameter. The sequence B was used for microgel superstructure formation and confocal imaging because it can be labelled using an $Atto_{565}$ fluorophore which, unlike SYBR gold, does not interact with the wavelength used for azobenzene actuation. Both sequences behave similarly in all conditions tested. Sequence A is identical to sequence $p(A_{20}$-

i-XL) from our previous publications and sequence B functions identically.[28] The role of each domain of the DNA sequence as well as the schematic representation of the DNA microgel formation is given Figure S2a. The sequence of the RCA product contains homoadenine runs that drives aggregation, a bare code domain for fluorescent labelling and a self-hybridizing sequences that forms supramolecular crosslink. Upon heating in presence of Magnesium (+II) or Clacium (+II) ions in solution the DNA strands form liquid coacervate due to the presence of the homoadenine runs. Upon cooling the self-hybridizing sequence forms supramolecular crosslinks which stabilize the DNA-rich phase against dissolution. As shown in Figure S2b, without compartmentalization the process yields polydisperse particles. A detailed protocol has already been published previously. The sequence B formed through the exact same mechanism since they only differ in terms of bare code domain.

4.4. Preparation and self-assembly of monodisperse microgels

Preparation of the microfluidic emulsion: First an homogeneous solution of RCA products was obtained by diluting the RCA product at 1.5 times the target concentration into 200 µL of into TE buffer and heating the solution up to 95 °C for 15 min for homogenization. Then then 30 µL of $CaCl_2$ solution at 500 mM and 70 µL of TE buffer are introduced in the mixture. The solution was used immediately for the preparation of the microfluidic emulsion. We used fluorinated Oil (Novec7500, 3M) supplemented with 2 % of a perfluoropolyether-polyethyleneglycol block-copolymer(PFPE-PEG-PFPE) as continuous phase. The preparation of the microfluidic devices made of poly-(dimethylsiloxane) (PDMS, Sylgard 184) and the synthesis of the block-copolymer surfactant were performed as previously reported.[50,51] The device consists of a flow-focusing junction with a 30x30x20 µm nozzle (Figure S3), where the aqueous and oil phase are respectively injected into the central and side channels. The solutions are injected using 1 mL syringes (Terumo) and PTFE tubing (Fisher Scientific) with an inner diameter of 0.3 mm and an outer diameter of 0.76 mm. The flow was controlled using a Nemesys syringe pumps (Cetoni). We typically used volumetric flows of 400 $\mu L.h^{-1}$ for the

DNA solution and 600 µL.h^{-1} for the fluorinated oil solution. The resulting emulsion contains 35 µm droplets which are directly gathered into a 1.5 mL microtube while the oil excess is removed continuously.

Arrested phase-separation in confinement: After production we covered the microfluidic emulsion using few drops of mineral oil to avoid evaporation. The tube was placed inside a temperature controlled heater (Thermomixer, Eppendorf) without agitation and heated for 2 h at 85 °C. After cooling down to room temperature, the microgels were either gathered via destabilisation of the microfluidic emulsion or imaged using fluorescence microscopy. For confocal imaging, we introduced 2 µL of SYBR gold (diluted at 100X into TE buffer) into 45 µL of emulsion and left the mixture overnight in the fridge for the dye diffuse across the organic phase.

Note that the assembly time is significantly longer than what was previously used. Indeed if when providing insufficient time for the phase separated compartment forming inside a single droplet to merge we obtained polydisperse DNA microgels. (Figure S4)

Gathering the monodisperse DNA microgels: To destabilize 100 µL of microfluidic emulsion we introduced 20 µL of 0.2 M EDTA solution, 10 µL of 1 % Triton X-100 solution, and 10 µL of perfluorooctanol. The mixture was then shaken vigourously and left 10 min on the bench top until the two phases become separated by a clear interface. The aqueous supernatant was then gathered in a separated tube. The particles were directly imaged by adding 5 µL of SYBR gold diluted 10 times in TE buffer to 50 µL of particle suspension.

For light driven actuation and superstructure assembly the DNA particles were washed three times by centrifugation at 2000 g for 10 min and redispession in fresh TE buffer. The concentration of the suspension obtained by redissolving 2 µL of DNA suspension diluted in 8 µL of TE (by heating at 95°C for 2 min) was measured by UV-vis spectroscopy. Finally we adjusted the stock microgel concentration to 200 mg.L^{-1} using TE buffer. For confocal microscopy experiments the DNA microgels were functionalized using 1 µL of 100 µM

fluorescent oligomer ($Atto_{565}$-B) for 10 µL of particle suspension at 200 $mg.L^{-1}$. The microgels were washed and redispersed in fresh TE a last time by centrifugation before use.

Superstructure assembly: Periodic microgel assemblies were obtained by drying a concentrated microgel suspension. Typically 20 µL of fluorescently labelled microgels suspension at 200 $mg.L^{-1}$ was concentrated to about 1 $g.L^{-1}$ by centrifugation. A drop of suspension was cast onto a glass slide and left to evaporate slowly at room temperature. Marangoni flow concentrate the microgels on the edge of the drop during evaporation and yield compact microgel assembly. Rehydrating the assemblies using a TE buffer containing 3 mM of magnesium yields periodic lattices of particles immobilized on the glass slides. On contrary, a treatment at 60 °C for 5 min followed by a rehydration using a TE buffer containing 0.1 % of Triton X100 yields free standing microgel films floating in solution. The AzoTAB, and if needed magnesium, are then introduced in solution for light driven actuation.

4.5. Light driven actuation

Preparation of a stock solution of trans-azoTAB: A 100 mM trans-azoTAB aqueous stock solution was prepared by dissolving an appropriate amount of the azobenzene derivative (M = 408.3 $g.mol^{-1}$) in Milli-Q water in an Eppendorf tube, and the pH adjusted to 8 with NaOH (0.1 M) or HCl (0.1 M). The stock solution was stored for three days in the dark before use to ensure complete isomerisation to the trans state, and then protected from light during use by wrapping the vial with aluminium foil.

Light intensities of LEDs: Optical intensities of the LEDs were measured with a silicon photodetector (model 918D-UV-OD3R, Newport Corporation, USA) along the emission axis at a distance of 5 cm from the light source (which was the typical distance used in all experiments). When not specified the intensities of UV and blue light irradiation were in the range of a few $mW.cm^{-2}$.

Light-actuated reversible swelling of DNA microgels: We first determined the influence of trans- and cis-azoTAB on the diameter of the DNA microgels as follows. DNA microgels were suspended in TE buffer or in 3-50 mM MgCl2 solution, then aliquots of trans-azoTAB stock solution or UV-adapted cis-azoTAB (prepared by irradiating the stock solution of trans-azoTAB with UV light for 15 minutes) were added to the microgels suspensions to reach final azoTAB concentrations comprised between 0.3 and 10 mM. The microgels were loaded into an observation chamber and left to settle for 5 minutes, then imaged by optical microscopy on a Leica DMI4000 inverted microscope using a ×63 oil immersion lens (HCX PL APO, 1.4 NA). The diameter of the microgels was measured using ImageJ on >20 microgels in the same field of view, and the average value and standard deviation reported.

Light-mediated swelling/compaction of the microgels was monitored on samples containing 3 mM azoTAB in TE buffer or in TE supplemented with 3 mM $MgCl_2$ solution. UV or blue light irradiation of the microgels was performed using external LEDs operating at 365 nm or 450 nm, respectively. On/off actuation was performed by alternatively turning on/off the UV and blue light sources. The diameter of the microgels was measured using ImageJ on >20 microgels in the same field of view, and the average value and standard deviation reported. Movies of microgels' swelling and compaction were acquired during irradiation using MicroManager and processed with ImageJ.

Light-actuated reversible swelling of DNA microgels: Light-responsive microgels were prepared by adding 3 mM trans-azoTAB to fluorescently labelled microgels. The suspension of trans-azoTAB-doped fluorescent microgels was then loaded into an observation chamber and the microgels were left to settle for 5 minutes. The microgels were imaged by confocal fluorescence microscopy on a Leica SPE confocal laser scanning microscope attached to a Leica DMIRE2 inverted microscope and equipped with a ×63 oil immersion lens (HCX PL APO, 1.4 NA). Excitation (and emission) wavelengths were set to 561 nm (emission: 575 – 675 nm) to monitor $Atto_{564}$ fluorescence. UV light irradiation was performed using an external

LEDs operating at 365 nm positioned at ~2 cm from the microscope slide. In comparison, blue light irradiation was performed using the in situ 488 nm wavelength of the confocal laser. On/off actuation was performed by alternatively turning on/off the UV and blue light sources. Z-stacks of the microgels were acquired using the built-in Leica Application Suite software and zy and xy projections obtained using ImageJ. Movies of microgels' swelling and compaction were acquired during irradiation using the built-in Leica Application Suite software and processed with ImageJ. The DNA superstructures were imaged by confocal microscopy during light-actuation using the same set-up as for the individual microgels (see above).

Supporting Information
Supporting Information is available from the Wiley Online Library or from the author.

Acknowledgements
This work was supported by LabEx AMADEus (ANR-10-LABX-42) in the framework of IdEx Bordeaux (ANR-10-445IDEX-03-02), France. JCB acknowledges the additional financial support of the Région Nouvelle Aquitaine. RM also thanks A. Walther and A. Samanta for providing a sample of DNA to start the project.

Received: ((will be filled in by the editorial staff))
Revised: ((will be filled in by the editorial staff))
Published online: ((will be filled in by the editorial staff))

References

[1] O. Erol, A. Pantula, W. Liu, D. H. Gracias, *Adv. Mater. Technol.* **2019**, *4*, 1900043.
[2] M. J. Buehler, R. Ballarini, Eds., *Materiomics: Multiscale Mechanics of Biological Materials and Structures*, Vol. 546, Springer Vienna, Vienna, **2013**.
[3] R. Merindol, A. Walther, *Chem. Soc. Rev.* **2017**, *46*, 5588.
[4] P. Cai, B. Hu, W. R. Leow, X. Wang, X. J. Loh, Y.-L. Wu, X. Chen, *Adv. Mater.* **2018**, *30*, 1800572.
[5] A. T. Blanchard, K. Salaita, *Science* **2019**, *365*, 1080.
[6] A. C. Daly, L. Riley, T. Segura, J. A. Burdick, *Nat. Rev. Mater.* **2020**, *5*, 20.
[7] N. C. Seeman, H. F. Sleiman, *Nat. Rev. Mater.* **2017**, *3*, 17068.
[8] M. R. Jones, N. C. Seeman, C. A. Mirkin, *Science* **2015**, *347*, 6224.
[9] J. B. Lee, Y. H. Roh, S. H. Um, H. Funabashi, W. Cheng, J. J. Cha, P. Kiatwuthinon, D. A. Muller, Dan. Luo, *Nat. Nanotechnol.* **2009**, *4*, 430.
[10] J. Y. Kishi, T. E. Schaus, N. Gopalkrishnan, F. Xuan, P. Yin, *Nat. Chem.* **2018**, *10*, 155.
[11] A. Padirac, T. Fujii, Y. Rondelez, *Proc. Natl. Acad. Sci. USA* **2012**, *109*, E3212.
[12] D. Y. Zhang, G. Seelig, *Nat. Chem.* **2011**, *3*, 103.
[13] F. Bomboi, F. Romano, M. Leo, J. Fernandez-Castanon, R. Cerbino, T. Bellini, F. Bordi, P. Filetici, Francesco. Sciortino, *Nat. Commun.* **2016**, *7*, 13191.
[14] E. Cheng, Y. Xing, P. Chen, Y. Yang, Y. Sun, D. Zhou, L. Xu, Q. Fan, D. Liu, *Angew. Chem. Int. Ed. Engl.* **2009**, *48*, 7660.

[15] Y. Hu, W. Guo, J. S. Kahn, M. A. Aleman-Garcia, I. Willner, *Angew. Chem. Int. Ed. Engl.* **2016**, *55*, 4210.
[16] Y. Helwa, N. Dave, R. Froidevaux, A. Samadi, J. Liu, *ACS Appl. Mater. Interfaces* **2012**, *4*, 2228.
[17] Z. Zhu, C. Wu, H. Liu, Y. Zou, X. Zhang, H. Kang, C. J. Yang, W. Tan, *Angew. Chem. Int. Ed. Engl.* **2010**, *49*, 1052.
[18] S. M. Douglas, I. Bachelet, G. M. Church, *Science* **2012**, *335*, 831.
[19] T. Fujii, Y. Rondelez, *ACS Nano* **2013**, *7*, 27.
[20] K. F. Wagenbauer, C. Sigl, H. Dietz, *Nature* **2017**, *552*, 78.
[21] L. L. Ong, N. Hanikel, O. K. Yaghi, C. Grun, M. T. Strauss, P. Bron, J. Lai-Kee-Him, F. Schueder, B. Wang, P. Wang, J. Y. Kishi, C. Myhrvold, A. Zhu, R. Jungmann, G. Bellot, Y. Ke, P. Yin, *Nature* **2017**, *552*, 72.
[22] J. B. Lee, S. Peng, D. Yang, Y. H. Roh, H. Funabashi, N. Park, E. J. Rice, L. Chen, R. Long, M. Wu, D. Luo, *Nat. Nanotechnol.* **2012**, *7*, 816.
[23] I. Michaeli, J. T. G. Overbeek, M. J. Voorn, *J. Polym. Sci.* **1957**, *23*, 443.
[24] N. Martin, *ChemBioChem* **2019**, *20*, 2553.
[25] T. Beneyton, C. Love, M. Girault, T.-Y. D. Tang, J.-C. Baret, *ChemSystemsChem* **2020**, *2*, e2000022.
[26] R. Galinis, G. Stonyte, V. Kiseliovas, R. Zilionis, S. Studer, D. Hilvert, A. Janulaitis, L. Mazutis, *Angew. Chem. Int. Ed. Engl.* **2016**, *55*, 3120.
[27] G. Zubaite, K. Simutis, R. Galinis, V. Milkus, V. Kiseliovas, L. Mazutis, *Micromachines* **2017**, *8*, 62.
[28] R. Merindol, S. Loescher, A. Samanta, A. Walther, *Nat. Nanotechnol.* **2018**, *13*, 730.
[29] Y. Wang, Y. Wang, X. Zheng, E. Ducrot, J. S. Yodh, M. Weck, D. J. Pine, É. Ducrot, J. S. Yodh, M. Weck, D. J. Pine, *Nat. Commun.* **2015**, *6*, 7253.
[30] É. Ducrot, M. He, G.-R. Yi, D. J. Pine, *Nat. Mater.* **2017**, *16*, 652.
[31] J. D. Debord, L. A. Lyon, *J. Phys. Chem. B* **2000**, *104*, 6327.
[32] A. Samanta, V. Sabatino, T. R. Ward, A. Walther, *Nature Nanotechnology* **2020**, *15*, 914.
[33] X. Du, Y. Bi, P. He, C. Wang, W. Guo, *Adv. Funct. Mater.* 2006305.
[34] L. Peng, M. You, Q. Yuan, C. Wu, D. Han, Y. Chen, Z. Zhong, J. Xue, W. Tan, *J. Am. Chem. Soc.* **2012**, *134*, 12302.
[35] Y. Zakrevskyy, M. Richter, S. Zakrevska, N. Lomadze, R. von Klitzing, S. Santer, *Adv. Funct. Mater.* **2012**, *22*, 5000.
[36] J. Li, C. Zheng, S. Cansiz, C. Wu, J. Xu, C. Cui, Y. Liu, W. Hou, Y. Wang, L. Zhang, I. -ting Teng, H.-H. Yang, W. Tan, *J. Am. Chem. Soc.* **2015**, *137*, 1412.
[37] A. Cangialosi, C. Yoon, J. Liu, Q. Huang, J. Guo, T. D. Nguyen, D. H. Gracias, R. Schulman, *Science* **2017**, *357*, 1126.
[38] J. Fern, R. Schulman, *Nat Commun* **2018**, *9*, 3766.
[39] M. Motornov, Y. Roiter, I. Tokarev, S. Minko, *Prog. Polym. Sci.* **2010**, *35*, 174.
[40] A.-L. M. Le Ny, C. T. Lee, *J. Am. Chem. Soc.* **2006**, *128*, 6400.
[41] A. Estévez-Torres, D. Baigl, *Soft Matter* **2011**, *7*, 6746.
[42] A. Estevez-Torres, C. Crozatier, A. Diguet, T. Hara, H. Saito, K. Yoshikawa, D. Baigl, *Proc. Natl. Acad. Sci. USA* **2009**, *106*, 12219.
[43] N. Martin, L. Tian, D. Spencer, A. Coutable‐Pennarun, J. L. R. Anderson, S. Mann, *Angew. Chem. Int. Ed. Engl.* **2019**, *58*, 14594.
[44] W. B. Rogers, V. N. Manoharan, *Science* **2015**, *347*, 639.
[45] E. Siéfert, E. Reyssat, J. Bico, B. Roman, *Nat. Mater.* **2019**, *18*, 24.
[46] N. Park, S. H. Um, H. Funabashi, J. F. Xu, D. Luo, *Nat. Mater.* **2009**, *8*, 432.
[47] W. Li, L. Zhang, X. Ge, B. Xu, W. Zhang, L. Qu, C.-H. Choi, J. Xu, A. Zhang, H. Lee, D. A. Weitz, *Chem. Soc. Rev.* **2018**, *47*, 5646.
[48] D. Dendukuri, P. S. Doyle, *Adv. Mater.* **2009**, *21*, 4071.

[49] N. Martin, K. P. Sharma, R. L. Harniman, R. M. Richardson, R. J. Hutchings, D. Alibhai, M. Li, S. Mann, *Sci. Rep.* **2017**, *7*, 1.
[50] T. Beneyton, I. P. M. Wijaya, P. Postros, M. Najah, P. Leblond, A. Couvent, E. Mayot, A. D. Griffiths, A. Drevelle, *Sci. Rep.* **2016**, *6*, 27223.
[51] T. Beneyton, D. Krafft, C. Bednarz, C. Kleineberg, C. Woelfer, I. Ivanov, T. Vidaković-Koch, K. Sundmacher, J.-C. Baret, *Nat. Commun.* **2018**, *9*, 2391.

Phase transition phenomenon are commonly used to synthesize and actuate synthetic hydrogels. We bring this concept into DNA materials to prepare monodisperse all-DNA microgels and embed them with light responsive properties. We use confined phase separation to control the size of the microgels and a photoresponsive surfactant to trigger 10-fold swelling within seconds on isolated microgels and periodic superstructures.

Rémi Merindol,*[a] Nicolas Martin,[b] Thomas Beneyton,[b] Jean-Christophe Baret,[b,c] and Serge Ravaine[b]

Fast and ample light controlled actuation of monodisperse all-DNA microgels

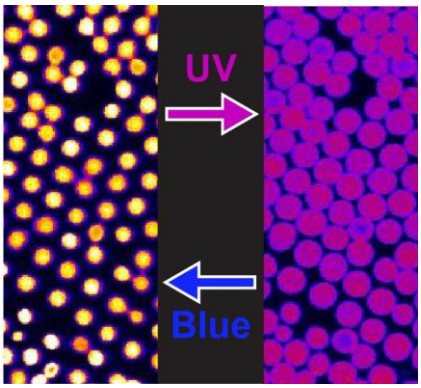

ToC figure

Supporting Information

Fast and ample light controlled actuation of monodisperse all-DNA microgels

Rémi Merindol,[a] Nicolas Martin,[b] Thomas Beneyton, [b] Jean-Christophe Baret,[b,c] and Serge Ravaine[b]*

Supplementary Movies

Movie S1. Optical microscopy video showing multiple swelling/compaction of *trans*-azoTAB-doped all-DNA microgels under alternating UV and blue light irradiation. Movie is shown at 5-time speed at 25 frames per second. Total duration of recording was 2 min in real time. Scale bar = 20 μm.

Movie S2. Confocal fluorescence microscopy video showing multiple swelling/compaction of *trans*-azoTAB-doped all-DNA $Atto_{565}$-labelled fluorescent microgels under alternating UV and blue light irradiation. False colouring using the Fire LUT is used. Movie is shown at 10-time speed at 12 frames per second. Total duration of recording was 2min in real time. Scale bar = 20 μm.

Movie S3 Confocal fluorescence microscopy video showing the swelling/compaction of an array of microgels immobilized ont a glass coverslip under alternating UV and blue light irradiation, showing changes in surface coverage. False colouring using the Fire LUT is used. Movie is shown at 10-time speed at 3.5 frames per second. Total duration of recording was 2 min in real time. Scale bar = 20 μm.

Movie S4. Confocal fluorescence microscopy video showing multiple swelling/compaction of a small free-standing DNA microgel film under alternating UV and blue light irradiation. False colouring using the Fire LUT is used. The focus is continuously adjusted in the z direction to keep the same microgels in the confocal plane. Movie is shown at 10-time speed at 12 frames per second. Total duration of recording was 2 min 30 s in real time. Scale bar = 10 μm.

Movie S5. Confocal fluorescence microscopy video showing multiple swelling/compaction of a larger free-standing DNA microgel film under alternating UV and blue light irradiation, showing large scale reconfigurations. False colouring using the Fire LUT is used. Movie is shown at 10-time speed at 3.5 frames per second. Total duration of recording was 6 min in real time. Scale bar = 20 μm.

Supplementary Figures

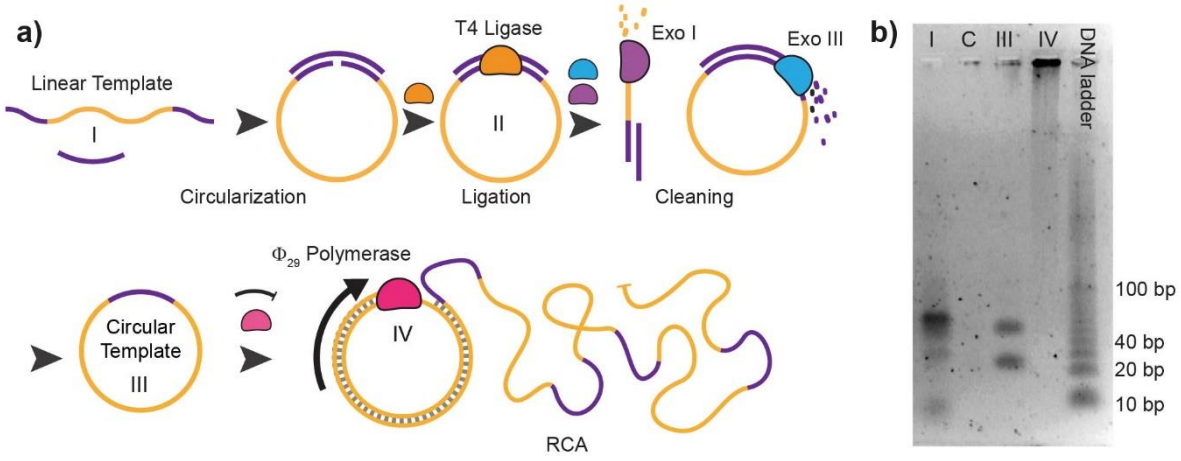

Figure S1. Rolling Circle Amplification. a) Schematic representation of the circularization of the linear template, their purification using exonucleases and the RCA of the purified templates. b) Gel electrophoresis (Agarose 2% in TBE, 5 $V.cm^{-1}$, 90 min) of the starting mixture of linear strands (I) of the purified circular template (III) and of the RCA product (IV). The control experiment (C) shows the full digestion of the linear templates by the exonucleases when we skipped ligation.

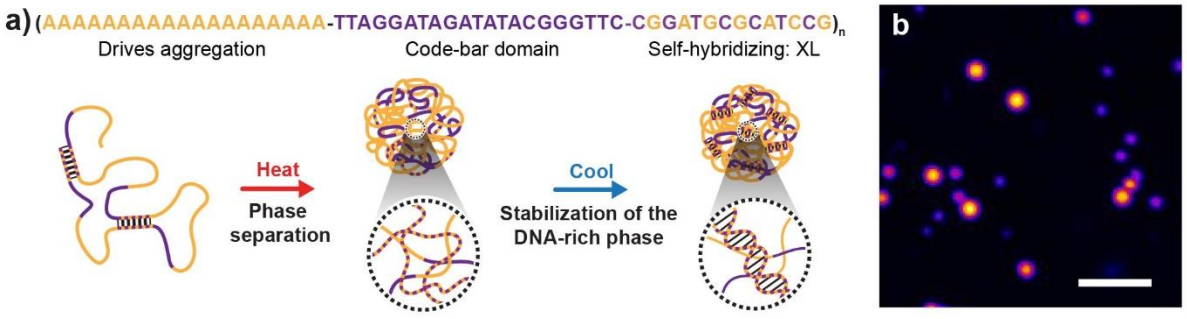

Figure S2. Arrested phase separation to form all-DNA microgels. a) Sequence of the RCA product A and schematic representation of the arrested phase separation that yield all-DNA microgels. The adenine run (yellow) drives phase separation at high temperature, the bare code domains (purple) serves to attach a fluorescent probe for CLSM, and the self-hybridizing domain (dashed) stabilize the DNA rich phase upon cooling which yields the DNA microgels.

b) Confocal Laser Scanning Micrograph (CLSM) imaging of the polydisperse microgels obtained after heating a 0.1 $g.L^{-1}$ solution of RCA product for 5 min at 85°C in 50 mM Ca^{2+}. The particles are made fluorescent by adding diluting SYBR gold (1 X) in the particle suspension. Scale bar is 10 µm.

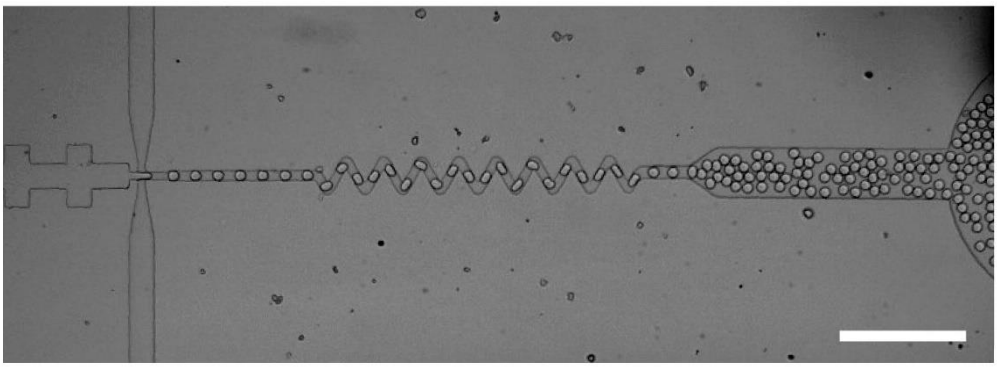

Figure S3. Optical micrograph showing the production of a monodisperse emulsion using a microfluidic T-junction. Oil flow 600 $\mu L.h^{-1}$, water flow 400 $\mu L.h^{-1}$. Scale Bar is 0.5 mm.

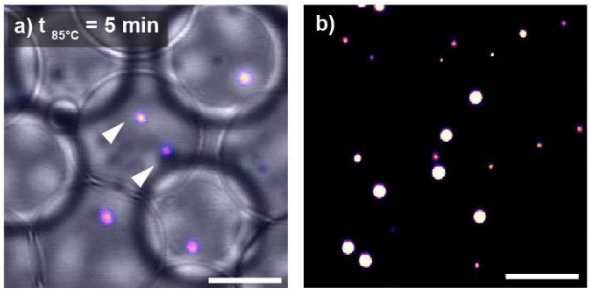

Figure S4. a) Superposition of CLSM and transmission optical micrographs showing two microgels in a single microfluidic drop after 5 min at 85 °C prepared from a DNA solution at 100 $mg.L^{-1}$. For such short time at high temperature the DNA rich phase does coalesce in a single domain which increases the polydispersity of the final microgels. b) CLSM showing both large monodisperse DNA microgels as well as smaller polydisperse microgels obtained after destabilization of the previous emulsion. Scale bars are 20 µm.

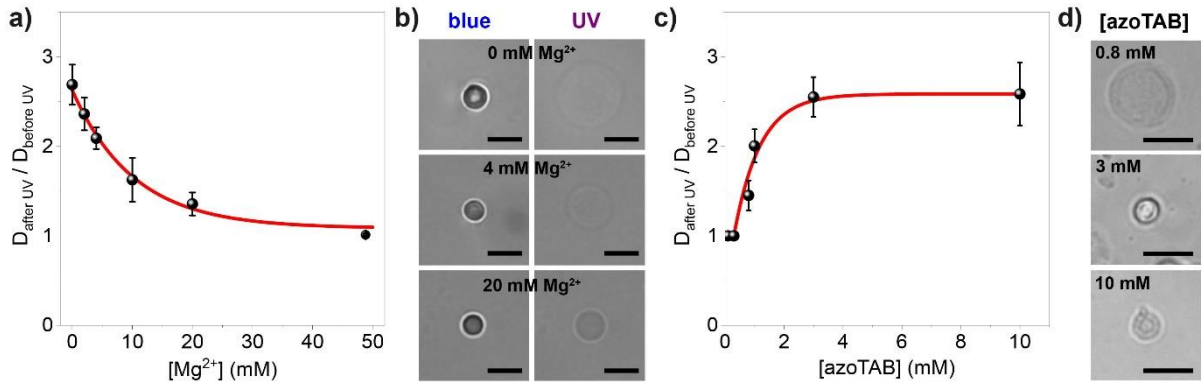

Figure S5. a) Graph presenting the evolution of the swelling ratio of the microgels under UV as function of the magnesium concentration. b) Optical micrographs showing the DNA microgels before and after swelling at different magnesium concentration (for 3 mM of azoTAB). The size of the swollen microgels decreases with increasing magnesium concentration, due to the higher ionic strength which decreases the swelling ratio. At 0mM Mg^{2+} the collapsed microgels are irregular. c) Graph presenting the evolution of the swelling ratio under UV as function of the azoTAB concentration (in absence of Mg^{2+}). d) Optical micrographs showing of the compact state of the DNA microgels as function of the azoTAB concentration. 3 mM of azoTAB is sufficient to collapse the DNA microgels and obtain the maximal swelling ratio. Error bars in a,c) represent the standard deviation from the average value measured on 10 droplets from the same field of view

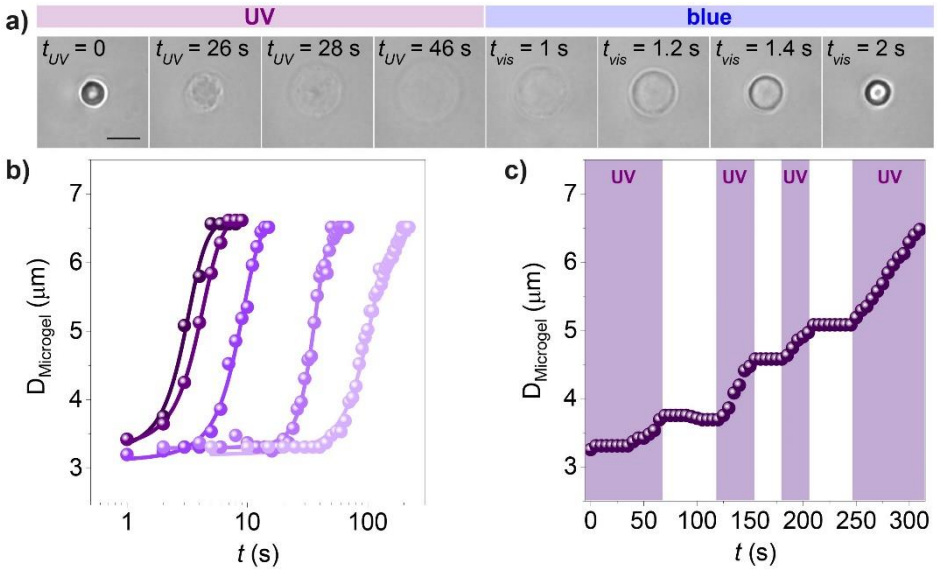

Figure 6. a) Temporal evolution of the swelling and deswelling of the DNA microgels respectively under UV and blue light irradiation (3mM azoTAB, no $MgCl_2$). b) Graph presenting the swelling speed of the DNA microgels as function of the UV-light intensity. The light intensity from left to right: 12.4 $mW.cm^{-2}$, 9.6 $mW.cm^{-2}$, 4.3 $mW.cm^{-2}$, 1.4 $mW.cm^{-2}$, and 0.8 $mW.cm^{-2}$. c) Temporal control of microgel swelling. Under UV light (purple bands, intensity 1.4 $mW.cm^{-2}$) the microgels swell and immediately stop once the light is off.